Effective interaction potential and superfluid–solid transition of spatially indirect excitons

2009 J. Phys. A: Math. Theor. 42 214016

(http://iopscience.iop.org/1751-8121/42/21/214016)

IOP PUBLISHING JOURNAL OF PHYSICS A: MATHEMATICAL AND THEORETICAL

J. Phys. A: Math. Theor. **42** (2009) 214016 (9pp) doi:10.1088/1751-8113/42/21/214016

Effective interaction potential and superfluid–solid transition of spatially indirect excitons

A Filinov[1,2], P Ludwig[1], M Bonitz[1] and Yu E Lozovik[2]

[1] Christian-Albrechts-Universität zu Kiel, Institut für Theoretische Physik und Astrophysik, Leibnizstrasse 15, 24098 Kiel, Germany
[2] Institute of Spectroscopy RAS, Moscow region, Troitsk, 142190, Russia

E-mail: filinov@theo-physik.uni-kiel.de

Received 16 October 2008, in final form 17 October 2008
Published 8 May 2009
Online at stacks.iop.org/JPhysA/42/214016

Abstract
Using an adiabatic approximation, we derive an effective interaction potential for spatially indirect excitons in quantum well structures. Using this potential and path integral Monte Carlo simulations, we study exciton crystallization and the quantum melting phase transition in a macroscopic system of 2D excitons. Furthermore, the superfluid fraction is calculated as a function of density and is shown to vanish upon crystallization.

PACS numbers: 67.10.Ba, 67.25.dj, 64.70.kg, 67.80.−s, 68.65.Fg

(Some figures in this article are in colour only in the electronic version)

1. Introduction

In recent decades, systems of indirect excitons have been extensively studied experimentally [1] due to the prospects to achieve superfluidity and Bose condensation. Promising set-ups which have been successful in controlling the many-exciton state are electron–hole bilayers, e.g. [2, 3], or single quantum wells (QWs) using the quantum Stark confinement (QSC). The latter will be studied in the present work. As was shown in [4], through the QSC one can simultaneously produce spatially indirect excitons and achieve their spatial localization. By varying the applied electric field, one can control the exciton coupling parameter—the ratio of the mutual exciton–exciton interaction to the confinement energy, as shown in our previous simulations for GaAs and ZnSe structures [4]. With the increase of inter-exciton coupling, a striking phenomenon is expected—spatial ordering of excitons into a crystalline lattice. This quantum phase transition has been recently studied by a path integral Monte Carlo (PIMC) method for *trapped finite* Coulomb systems [5], systems of particles with dipole interaction [6] and symmetric electron–hole bilayers [2, 3, 7, 8]. Analytical results for the crystal phase have also been reported [9].

In the case of interacting Bose particles, in addition, (partial) superfluidity is expected. Then during the crystallization transition, one expects a gradual decrease of the superfluid

fraction. This behaviour has recently been studied in detail by PIMC simulations for Bose particles with the Coulomb interaction [10]. It was shown that the superfluid density can be concentrated either in the core or at the cluster boundary depending on the hexagonal order in the clusters which sensitively depends on the particle number. Furthermore, a two-dimensional *homogeneous* dipole system of up to 400 particles has recently been studied [11, 12]. The crystallization point has been identified in ground state calculations (DMC) by comparing the energies of the solid and gas phases [11], and by a break of the translational symmetry of the pair distribution functions (PDFs) and abrupt vanishing of the superfluid fraction at this point [12]. The authors found a transition point at a density of $nr_0^2 = 290 \pm 30$ or $D = \sqrt{n}r_0 = 17 \pm 1$ (with r_0 being the characteristic distance defined by the relevant energy scales, $\hbar^2/mr_0^2 = e^2d^2/4\pi\epsilon r_0^3$). In the present paper, we test the validity of the dipole model for indirect excitons. In fact, the effective exciton–exciton interaction V_{xx} is a quantum-mechanical four-body problem which has been studied, e.g., by Zimmermann and Schindler [13] and may significantly deviate from the simple dipole form at distances comparable with the exciton dipole length. We, therefore, devote special care to compute V_{xx} from first-principle PIMC simulations. We find that this interaction allows for a second-phase transition—quantum melting of the exciton crystal by compression—missing in dipole systems. Further, we found that for an effective exciton dipole length below $d \lesssim 6a_{\mathrm{B}}^*$, the crystalline phase vanishes.

Below we present results for a model similar to the experimental set-up of the Timofeev group [14]: a single ZnSe-based QW with indirect excitons produced by an electric field [4] applied normal to a QW plane. In order to be able to perform simulations for a macroscopic ensemble of indirect excitons, we apply a bosonic model. As shown by various groups [15, 16], in the moderate density regime, the excitons are adequately treated as a composite particle obeying Bose statistics due to strong attractive interaction between the electrons and holes. In the simulations of [16], we were able to test this approximation against the exact two-component fermion system in a broad range of densities. In particular, we found that the bosonic model gives accurate predictions for the superfluid fraction once the excitons are in a strongly coupled–low/moderate-density regime. In contrast, in the weakly coupled–high-density regime close to or beyond the Mott density, the results are strongly affected by the Fermi statistics and the bosonic approximation breaks down. Thus, in the present analysis of moderate-density systems the bosonic model works well allowing us to study relatively large exciton ensembles without being hampered by the *fermion sign* problem.

2. Model

The general Hamiltonian for a system of N_{e} electrons and N_{h} holes ($N = N_{\mathrm{e}} + N_{\mathrm{h}}$) in the quantum well confinement and electric field can be written as

$$\hat{H}_{3\mathrm{D}} = \hat{H}_{\parallel}^{\mathrm{single}} + \hat{H}_{z}^{\mathrm{single}} + W, \tag{1}$$

with the *single* particle and *interaction* parts being defined as

$$\begin{aligned}
\hat{H}_{\parallel}^{\mathrm{single}} &= \sum_{i=1}^{N}\left[-\frac{\hbar^2}{2m_{\mathrm{e(h)}}^{\parallel}}\nabla_{\mathbf{r}_i}^2\right],\\
\hat{H}_{z}^{\mathrm{single}} &= \sum_{i=1}^{N}\left[-\frac{\hbar^2}{2m_{\mathrm{e(h)}}^{\perp}}\nabla_{z_i}^2 + V_{\mathrm{e(h)}}^{QW}(z_i) + V_{\mathrm{e(h)}}^{F}\{E_z(\mathbf{r}_i, z_i)\}\right],\\
W &= \sum_{i<j}^{N} V_{ij}^{\mathrm{Coul}}, \qquad V_{ij}^{\mathrm{Coul}} = \frac{e_i e_j}{\epsilon}[(\mathbf{r}_i - \mathbf{r}_j)^2 + (z_i - z_j)^2]^{-1/2}.
\end{aligned} \tag{2}$$

We consider a homogeneous electric field $E_z(\mathbf{r}_i, z_i) = E_z(z_i)$, where vectors $\mathbf{r}$ denote 2D vectors in the QW plane, V^{QW} is the QW confinement, V^{F} is the electrostatic potential energy due to the electric field and ϵ is the background dielectric constant.

To apply the approximation of bosonic excitons valid for low-to-moderate densities [16], we want to reduce the 3D Hamiltonian (1) to a 2D one, where all effects related to a particular width of the QW and the electric field strength will be combined in an effective inter-exciton interaction $V_{\mathrm{xx}}(R)$. This becomes possible by using the adiabatic approximation [17, 18]. This approach is justified for high values of the electric field E_z which leads to a strong localization of electrons and holes at opposite edges of the QW. To be specific, the calculations below correspond to $L = 30, \ldots, 120$ nm wide ZnSe QWs and $E_z = 20$ kV. Assuming the relation of energy scales, $\Delta\epsilon_i^{\mathrm{single}} \gg U^{\mathrm{int}}_{\mathrm{eh(ee,hh)}}$, where $\Delta\epsilon_i^{\mathrm{single}}$ is the characteristic spacing of the quantized one-particle energy levels in the z-direction and U^{int} is the interaction energy, we separate the out-of-plane motion and solve the 3D Bloch equation for the N-particle density matrix ρ_{3D}:

$$-\frac{\partial\hat{\rho}_{\mathrm{3D}}(\beta)}{\partial\beta} = \hat{H}_{\mathrm{3D}}\hat{\rho}_{\mathrm{3D}}(\beta) \tag{3}$$

in the adiabatic approximation, i.e.

$$\rho_{\mathrm{3D}}(\beta) = \rho_{\mathrm{2D}}(\mathbf{r}_1, \ldots, \mathbf{r}_N, \beta)\prod_{i=1}^{N_{\mathrm{e}}}\rho_{\mathrm{e}}(z_i, \beta)\prod_{j=1}^{N_{\mathrm{h}}}\rho_{\mathrm{h}}(z_j, \beta), \tag{4}$$

where $\beta = 1/k_{\mathrm{B}}T$ (below, we drop the argument β). Now integrating out in equation (3) all z-dependences, i.e. applying $\int\prod_{i=1}^{N_{\mathrm{e}}}\mathrm{d}z_i\prod_{j=1}^{N_{\mathrm{h}}}\mathrm{d}z_j$, we obtain a reduced 2D Bloch equation:

$$-\frac{\partial\rho_{\mathrm{2D}}}{\partial\beta} = \left(\sum_{i=1}^{N}-\frac{\hbar^2}{2m^{\parallel}_{\mathrm{e(h)}}}\nabla^2_{\mathbf{r}_i} + \sum_{i<j}^{N}\tilde{V}_{\alpha_i\beta_j}(r_{ij}) + \sum_{i=1}^{N}\epsilon_i^{\mathrm{single}}\right)\rho_{\mathrm{2D}}, \tag{5}$$

where we introduced a smoothened Coulomb potential:

$$\tilde{V}_{\alpha_i\beta_j}(r_{ij}) = \int V_{ij}^{\mathrm{Coul}}\rho_{\alpha_i}(z_i)\rho_{\beta_j}(z_j)\,\mathrm{d}z_i\,\mathrm{d}z_j, \qquad \alpha, \beta = e, h. \tag{6}$$

The densities $\rho_{\mathrm{e}}(z_{\mathrm{e}})$ and $\rho_{\mathrm{h}}(z_{\mathrm{h}})$ are found by solving a single-exciton problem in an electric field [17]. Also the exciton dipole moment, $\mu = e \cdot d$, follows directly from the electron and hole densities:

$$d = \langle z_{\mathrm{e}}\rangle - \langle z_{\mathrm{h}}\rangle = \int z_{\mathrm{e}}\rho_{\mathrm{e}}(z_{\mathrm{e}})\,\mathrm{d}z_{\mathrm{e}} - \int z_{\mathrm{h}}\rho_{\mathrm{h}}(z_{\mathrm{h}})\,\mathrm{d}z_{\mathrm{h}}. \tag{7}$$

The low-to-moderate density regime considered here also leads to another relation of energy scales, i.e. $E_{\mathrm{B}}(X) \gg V_{\mathrm{xx}}, k_{\mathrm{B}}T$, where E_{B} is the exciton binding energy. Under these conditions, the excitons remain in their internal quantum states described by a two-body density matrix $\rho^{\mathrm{ex}}(\mathbf{r}_{\mathrm{eh}})$ throughout their interaction. This pair density matrix depends on the electron–hole separation $\mathbf{r}_{\mathrm{eh}} = \mathbf{r}_{\mathrm{e}} - \mathbf{r}_{\mathrm{h}}$ and can be obtained numerically, e.g. with the matrix-squaring technique [19] applied to the interaction potential (6). Again using the adiabatic approximation (now in the 2D plane), we write ρ_{2D} as a product of a density matrix of an N_x particle complex and relative density matrices ρ^{ex} of N_x excitons:

$$\rho_{\mathrm{2D}} = \rho_{\mathrm{2D}}(\mathbf{R}^1, \ldots, \mathbf{R}^{N_x})\prod_{a=1}^{N_x}\rho^{\mathrm{ex}}\left(r^a_{\mathrm{eh}}\right). \tag{8}$$

Here we have assumed electrical neutrality, $N_{\mathrm{e}} = N_{\mathrm{h}} = N_x$, and introduced the electron–hole pair coordinates related to the same exciton, $(\mathbf{r}_1, \ldots, \mathbf{r}_N) = \left\{\left(\mathbf{r}^a_{\mathrm{e}}, \mathbf{r}^a_{\mathrm{h}}\right) = \left(\mathbf{R}^a, \mathbf{r}^a_{\mathrm{eh}}\right)\right\}\big|_{a=1,\ldots,N_x}$,

with the centre-of-mass (c.o.m.) coordinates $\mathbf{R}^a = \left(m_e^{\parallel}\mathbf{r}_e^a + m_h^{\parallel}\mathbf{r}_h^a\right)/M_x$, $M_x = m_e^{\parallel} + m_h^{\parallel}$. Certainly, the ansatz (8) implies that the excitons are stable against external perturbations and we are below the Mott density.

Now averaging equation (5) over the relative degrees of freedom of excitons, i.e. integrating over $\int \prod_{a=1}^{N_x} \mathrm{d}\mathbf{r}_{eh}^a$, we obtain the N_x-exciton Bloch equation depending on the c.o.m. coordinates:

$$-\frac{\partial \rho_{2D}(\mathbf{R}^1, \ldots, \mathbf{R}^{N_x})}{\partial \beta} = (\hat{H}^{\mathrm{eff}} + E_x)\rho_{2D}(\mathbf{R}^1, \ldots, \mathbf{R}^{N_x}), \tag{9}$$

$$\hat{H}^{\mathrm{eff}} = \sum_{a=1}^{N_x} -\frac{\hbar^2}{2M_x}\nabla_{\mathbf{R}^a}^2 + \sum_{a<b}^{N_x} V_{\mathrm{xx}}(R^{ab}), \tag{10}$$

$$E_x = \sum_{a=1}^{N_x} \left\langle -\frac{\hbar^2}{2\mu_x}\nabla_{\mathbf{r}_{eh}^a}^2 + \tilde{V}_{eh}\left(r_{eh}^a\right)\right\rangle_{\rho^{\mathrm{ex}}} + \sum_{i=1}^{N} \epsilon_i^{\mathrm{single}}. \tag{11}$$

The interaction term in the *effective exciton* Hamiltonian $\hat{H}^{\mathrm{eff}}$ is defined as the sum of the effective (adiabatically averaged) interactions of two electrons and two holes in excitons a and b ($a \neq b$):

$$V_{\mathrm{xx}}(R^{ab}) = \int \sum_{\alpha,\beta=e,h} \tilde{V}_{\alpha\beta}\left(\left|\mathbf{r}_\alpha^a - \mathbf{r}_\beta^b\right|\right)\rho^{\mathrm{ex}}\left(r_{eh}^a\right)\rho^{\mathrm{ex}}\left(r_{eh}^b\right)\mathrm{d}\mathbf{r}_{eh}^a\,\mathrm{d}\mathbf{r}_{eh}^b. \tag{12}$$

The distances of two particles from different excitons can be expressed as

$$\begin{aligned}
\mathbf{r}_h^a - \mathbf{r}_h^b &= \mathbf{R}^a - \mathbf{R}^b + m_e\left(\mathbf{r}_{eh}^a - \mathbf{r}_{eh}^b\right)/M_x,\\
\mathbf{r}_e^a - \mathbf{r}_e^b &= \mathbf{R}^a - \mathbf{R}^b - m_h\left(\mathbf{r}_{eh}^a - \mathbf{r}_{eh}^b\right)/M_x,\\
\mathbf{r}_h^a - \mathbf{r}_e^b &= \mathbf{R}^a - \mathbf{R}^b + \left(m_e\mathbf{r}_{eh}^a + m_h\mathbf{r}_{eh}^b\right)/M_x.
\end{aligned} \tag{13}$$

After integration, in equation (12), only the c.o.m. dependence on $R^{ab} = |\mathbf{R}^a - \mathbf{R}^b|$ remains.

Thus, we have derived the effective Hamiltonian (10) of composite particles. The interaction potential (12) generalizes the dipole potential used in the previous analysis of spatially indirect excitons [6, 11, 12]. The comparison of both is discussed below. The corresponding N-body problem (10) can be solved with the path integral Monte Carlo technique which allows for a direct treatment of many-body correlation and bosonic exchange effects; for details, see [20–22].

3. Results

We have performed PIMC simulations for a 2D homogeneous system with $N = 60$ and 90 bosonic excitons in a simulation box with periodic boundary conditions. The potential (12) has been divided into a short- and long-range part, $V_{\mathrm{xx}} = (V_{\mathrm{xx}} - V_{\mathrm{D}}) + V_{\mathrm{D}}$, with the dipole interaction, $V_{\mathrm{D}} = (ed)^2/\epsilon r^3$, treated by the usual Ewald summation technique. We used the following system of units: $r \to r/a_{\mathrm{B}}^*$, $E \to E/\mathrm{Ha}^*$, with the electron Bohr radius, $a_{\mathrm{B}}^* = \hbar^2\epsilon/m_e^{\parallel}e^2$, and the electron Hartree, $\mathrm{Ha}^* = e^2/\epsilon a_{\mathrm{B}}^*$. Here, $M_x = m_e^{\parallel} + m_h^{\parallel}$ is the exciton mass. Parameters for typical semiconductor structures are listed in table 1. As it follows from the derivation in adiabatic approximation, the Hamiltonian (10) contains only the in-plane particles masses, $m_{e(h)}^{\parallel}$. The anisotropy of the parabolic bands for both electrons and holes, i.e. the out-of-plane effective masses, $m_{e(h)}^{\perp}$, are involved in the exciton solution in the z-direction. These masses determine the shape of the density matrices $\rho_e(z_e)$, $\rho_h(z_h)$ and

Table 1. Semiconductor QW parameters. Masses are in units of the free electron mass m_0. We consider an anisotropic hole mass in GaAs according to [24] which provides better agreement between theory and experiment for the exciton binding energy (see e.g. [18] and references therein).

	GaAs/AlGaAs	ZnSe/ZnSSe
ϵ	12.58	8.7
$m_{\mathrm{e}}^{\parallel}$	0.0667	0.15
$m_{\mathrm{h}}^{\parallel}$	0.112	0.37
$m_{\mathrm{h}}^{\perp}$	0.377	0.86
$M_x/m_{\mathrm{e}}^{\parallel}$	2.68	3.46
a_{B}^{*} (nm)	9.98	3.07
$H\mathrm{a}^{*}$ (meV)	11.47	53.93

hence indirectly influence the effective inter-exciton interaction via equation (6). In particular, for a 20 kV cm^{-1} electric field applied to a 30 nm wide QW the calculations of [4, 17] predict that the e–h separation (7) equals $d = 15.78$ nm for GaAs and $d = 20.41$ nm for ZnSe structures. Now comparing the ratio $\tilde{d} = d/a_{\mathrm{B}}^{*}$ for both structures, we find $\tilde{d} = 1.58$ and $\tilde{d} = 6.65$, respectively. This shows that in a ZnSe QW, the excitons are more strongly coupled and it is easy to reach a crystalline regime as discussed below. Other advantages of using materials with larger effective masses are (a) increased stability of excitons due to higher binding energies and (b) increased exciton lifetime due to a better separation of carriers in the z-direction (the radiative lifetime depends on the overlap of the density matrices $\rho_{\mathrm{e(h)}}(z_{\mathrm{e(h)}})$).

In the following we, therefore, concentrate on the ZnSe structure. However, the results presented in the dimensionless units, r/a_{B}^{*} and E/Ha^{*}, using table 1 can be applied to other materials as well. In particular, the effective potential V_{xx} (12) already reduces to a dipole interaction $V_{\mathrm{D}} = (ed)^2/\epsilon r^3$ at distances of about several exciton dipole moments d. In this case, the Hamiltonian (10) can be brought to a universal dimensionless form using the scale [12]: $a_0 = 1/\sqrt{n}$, $E_0 = \hbar^2/M_x a_0^2$. Both systems of units are connected via relations

$$
\begin{aligned}
&n = \frac{1}{a_0^2} = \frac{1}{\pi \bar{r}^2}, \qquad a_0 = \sqrt{\pi} r_s a_{\mathrm{B}}^{*}, \qquad r_s = \bar{r}/a_{\mathrm{B}}^{*},\\
&D = \frac{e^2 d^2}{\epsilon a_0^3 E_0} = \left(\frac{M_x}{m_{\mathrm{e}}^{\parallel}}\right) \tilde{d}^2 \frac{1}{\sqrt{\pi} r_s}, \qquad \tilde{d} = d/a_{\mathrm{B}}^{*},\\
&\frac{E_0}{H\mathrm{a}^{*}} = \left(\frac{m_{\mathrm{e}}^{\parallel}}{M_x}\right) \frac{1}{\pi r_s^2},
\end{aligned}
\tag{14}
$$

where $n = N/(L_x L_y)$ is the number density.

In figure 1, we show $V_{\mathrm{xx}}(r)[\mathrm{Ha}^{*}]$ for several e–h separations, $\tilde{d} = d_0, 2d_0, 3d_0, 4d_0$ with $d_0 = 6.64848$ ($\tilde{d} = d_0$ corresponds to a 30 nm ZnSe QW and field strength 20 kV cm^{-1}). In the right part we show, in addition, the dipole potential V_{D} and the classical exciton pair potential (limit of $\tilde{d} \ll r$), $V_{\mathrm{ex}} = 2/r - 2/\sqrt{r^2 + \tilde{d}^2}$. While at large distances V_{xx} agrees with V_{D}, for $r \lesssim 4\tilde{d}$, V_{xx} is substantially weaker. Further, as one might expect from the dipole model, overall the interaction is stronger with increasing d. However, at small distances, $r < 6a_{\mathrm{B}}^{*}$, V_{xx} shows the opposite behaviour which originates from the smoothening procedure (12) over the exciton relative density matrices: with an increase of $\tilde{d}$, e–h pairs become more weakly bound and the exciton in-plane size increases. This delocalization reduces the strength of the Coulomb interaction between two electrons and two holes, i.e. between two excitons.

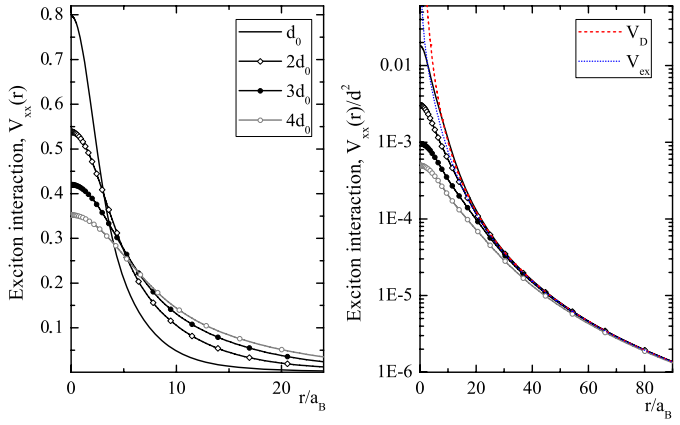

Figure 1. Left: exciton interaction potential $V_{xx}(r)$[Ha*] (equation (12)) for several dipole moments $\tilde{d}$. Right: $V_{xx}/\tilde{d}^2$ compared with the dipole potential, $V_D(r) = 1/r^3$, and classical exciton potential, $V_{ex} = (2/r - 2/\sqrt{r^2 + \tilde{d}^2})/\tilde{d}^2$ (shown for $\tilde{d} = d_0$).

Conversely, the stronger the binding of an e–h pair and its spatial localization, the faster V_{xx} approaches V_{ex}.

Let us now analyse the melting behaviour of the exciton ensemble. In [11, 12], the crystallization of dipoles was observed at $D = 17 \pm 1$. We now perform a similar analysis with the improved model interaction $V_{xx}(r)$, for $T = 1/3000$ Ha and consider a density range of $\rho a_B^{*2} = 1/\pi r_s^2$, $r_s = 5, \ldots, 12$. Simulations were performed for $\tilde{d}[d_0] = 1, 2, 3, 4$, and the results are shown in figures 2 and 3. At low densities where our potential is close to a dipole potential, we observe similar results as in [11, 12], i.e. crystallization of dipoles upon compression (not shown). But most importantly, at high density, we observe completely different behaviour which is due to the weak potential at small r: the exciton crystal melts upon compression. This transition is clearly seen from the 2D PDF in figure 2 (left) where an abrupt loss of a (quasi) long-range crystalline order is observed by a slight change in r_s from 10 (top) to 9.5 (bottom). Simultaneously, in figure 2 (right) we observe a topological change in the picture of the particle trajectories in the path integral representation [20]. While in the solid phase we observe only local exchanges of few particles, just after the melting transition the trajectories form macroscopically large permutation cycles crossing the edges of our periodic simulation cell. From the statistics of the flux of paths winding around the periodic cell, one can estimate the fraction of the superfluid density [20, 23]:

$$\gamma_s = \rho_s/\rho = M_x\langle W^2\rangle/\hbar^2\beta N_x, \qquad \mathbf{W} = \sum_{i=1}^{N_x}\int_0^\beta \mathrm{d}t\,[\mathrm{d}\mathbf{r}_i(t)/\mathrm{d}t]\,. \tag{15}$$

Figure 3 indicates a step-like increase of the superfluid density from zero up to about 35% in the gas phase. The vertical dotted line shows the Mott density where the excitons pressure ionize and the bosonic model fails. The critical values r_s^{ex} for the exciton quantum melting transition at different $\tilde{d}$ are collected in table 2 together with the critical data r_s^d for the dipole crystallization.

In conclusion, the derived exciton–exciton potential leads to completely different predictions for the phase diagram of bosonic excitons compared to the dipole model. Due to the much softer Coulomb-like interaction at small distances, the exciton solid melts by compression, similar to a Wigner crystal of electrons [5]. Due to this fact, it becomes possible

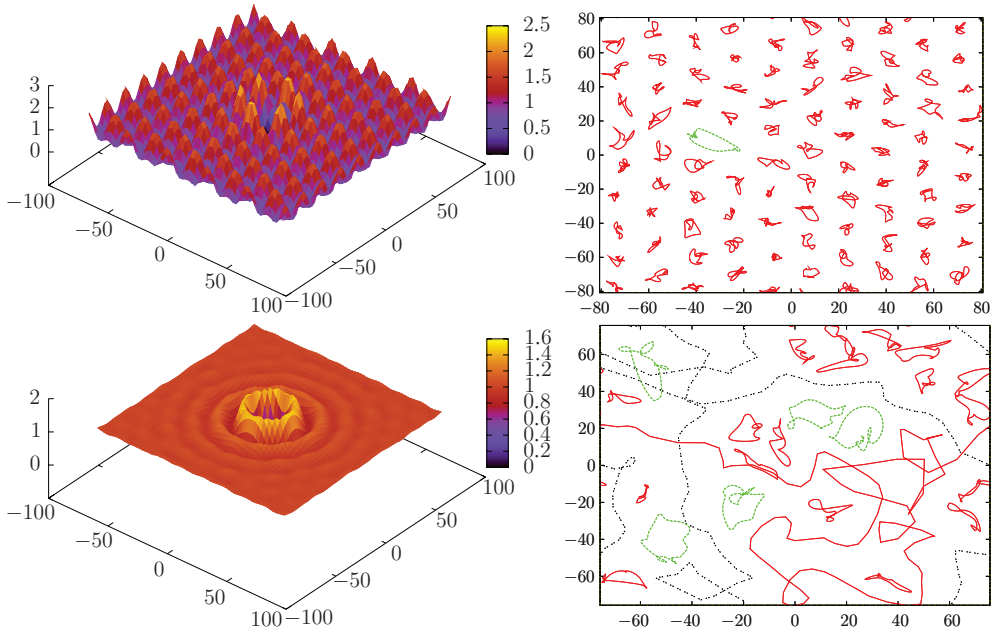

Figure 2. Left: 2D pair distribution function at $r_s = 10.0$ (top) in the solid and $r_s = 9.5$ (bottom) in the superfluid gas phase. Right: snapshots from PIMC simulations. The trajectories of particles involved in permutations of different lengths are denoted with different colours. $\tilde{d} = 3d_0$.

Table 2. Interparticle distances at first r_s^{d} and second r_s^{ex} phase transitions: superfluid gas–exciton solid. r_s^{d} are estimated from (14) and $D \geqslant 17 \pm 1$; r_s^{ex} are the PIMC results using $V_{\mathrm{xx}}(r)$ in figure 1. The exciton solid exists for densities $na_{\mathrm{B}}^{*2} = 1/\pi r_s^2$, with $r_s^{\mathrm{ex}} \leqslant r_s \leqslant r_s^{\mathrm{d}}$. The second column, L, is the required ZnSe QW width at the field strength $E_z = 20\,\mathrm{kV\,cm^{-1}}$.

$\tilde{d}(d_0)$	L (nm)	r_s^{d}	r_s^{ex}
1	30	5.1 (0.3)	–
2	∼50	20.4 (1.2)	10.0 (0.5)
3	∼70	45.90 (2.7)	10.0 (0.5)
4	∼90	81.6 (4.8)	11.0 (0.5)

to stabilize the exciton lattice only in a finite density interval (see table 2). Outside of this region, the excitons exist in a superfluid gas phase.

Several heterostructures are candidates for the observed effect, but ZnSe is favourable due to its relatively high value of the dipole moment. Using parameters from table 1 we estimate the exciton solid to exist in ZnSe (taking $\tilde{d} = 2d_0$) in a QW with $L \sim 50$ nm between $0.81 \leqslant \rho(10^{10}\,\mathrm{cm^{-2}}) \leqslant 3.38$ and $T \lesssim 2$ K and in GaAs in a QW with $L \sim 148$ nm between $0.77 \leqslant \rho(10^{9}\,\mathrm{cm^{-2}}) \leqslant 3.2$ and $T \lesssim 0.4$ K. While we have not considered disorder effects due to the imperfections of the QW planes, they can be important. In our case of the electric-field-induced indirect excitons, electrons and holes are pushed to the QW edges and hence experience the influence of QW width fluctuations and impurities [18]. This, on one hand, stabilizes the excitons [25]. On the other hand, as in the case of the electron Wigner crystal, this can additionally stabilize the exciton solid at high densities.

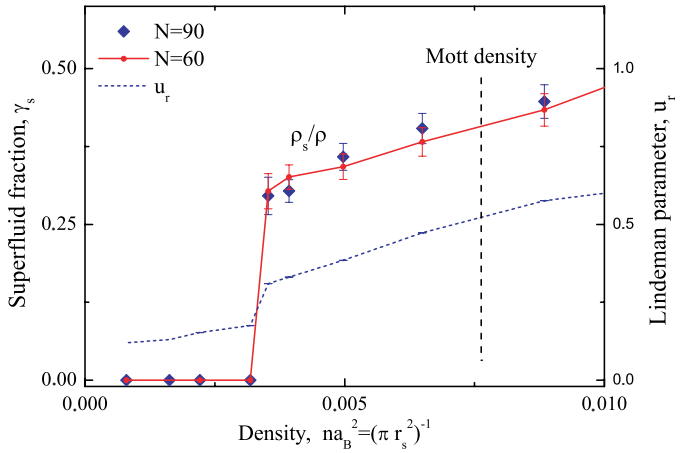

Figure 3. Superfluid fraction versus density na_B^{*2}, for $N = 60$ (circles) and $N = 90$ (diamonds) for $\tilde{d} = 3d_0$. The dotted line shows the Lindemann parameter u_r. The vertical line indicates the Mott density. The Bose model (superfluid data) is applicable only at lower densities [16].

Acknowledgments

Financial support by the Deutsche Forschungsgemeinschaft via SFB-TR24 grant A7 and FI 1252 is gratefully acknowledged.

References

[1] Negotia V *et al* 1999 *Phys. Rev* B **60** 2661
Butov L *et al* 2002 *Nature* **417** 47
Hammack A *et al* 2006 *Phys. Rev Lett.* **96** 227402 and references therein
[2] De Palo S, Rapisarda F and Senatore G 2002 *Phys. Rev. Lett.* **88** 206401
[3] Ludwig P, Balzer K, Filinov A, Stolz H and Bonitz M 2008 *New J. Phys.* **10** 083031
[4] Ludwig P, Filinov A, Bonitz M and Stolz H 2006 *Phys. Status Solidi* b **243** 2363
Sperlich K, Ludwig P, Filinov A, Bonitz M, Stolz H, Hommel D and Gust A 2009 *Phys. Status Solidi* c **6** 551
[5] Filinov A, Bonitz M and Lozovik Yu 2001 *Phys. Rev. Lett.* **86** 3851
Filinov A, Bonitz M and Lozovik Yu 2000 *Phys. Status Solidi* b **221** 231
[6] Lozovik Yu, Volkov S and Willander M 2004 *JETP Lett.* **79** 473
[7] Liu L, S'wierkowski L, Neilson D and Szyman'ski J 1996 *Phys. Rev.* B **53** 7923
Thakur J and Neilson D 1997 *Phys. Rev.* B **56** 10297
[8] Filinov A *et al* 2003 *J. Phys. A: Math. Gen.* **36** 5899
Filinov A *et al* 2003 *Phys. Status Solidi* c **5** 15182
Ludwig P, Filinov A, Lozovik Yu, Stolz H and Bonitz M 2007 *Contrib. Plasma Phys.* **47** 335
[9] Balzer K, Nölle C, Bonitz M and Filinov A 2006 *Phys. Status Solidi* c **3** 2402
Balzer K, Nölle C, Bonitz M and Filinov A 2006 *J. Phys.: Conf. Ser.* **35** 209
[10] Filinov A, Böning J, Bonitz M and Lozovik Yu 2008 *Phys. Rev.* B **77** 214527
[11] Astrakharchik G *et al* 2007 *Phys. Rev. Lett.* **98** 060405
[12] Büchler H *et al* 2007 *Phys. Rev. Lett.* **98** 060404
[13] Zimmermann R and Schindler C 2007 *Solid State Commun.* **144** 395
[14] Timofeev V *et al* 2007 *J. Phys.: Condens. Matter* **19** 295209
[15] Shumway J and Ceperley D 2000 *J. Phys. IV France* **10** Pr5–3
[16] Filinov A, Bonitz M, Ludwig P and Lozovik Yu E 2006 *Phys. Status Solidi* c **3** 2457
[17] Filinov A, Ludwig P, Lozovik Yu, Bonitz M and Stolz H 2006 *J. Phys.: Conf. Ser.* **35** 197
[18] Filinov A *et al* 2004 *Phys. Rev.* B **70** 35323
Bracker A *et al* 2005 *Phys. Rev.* B **72** 035332

[19] Storer R 1968 *J. Math. Phys.* **9** 964
Klemm A and Storer R 1973 *Aust. J. Phys.* **26** 43
[20] Ceperley D 1999 *Rev. Mod. Phys.* **71** 438
[21] Boninsegni M, Prokof'ev N and Svistunov B 2006 *Phys. Rev. Lett.* **96** 070601
[22] Bonitz M and Semkat (eds) D 2006 *Introduction to Computational Methods for Many-Body Physics* (Princeton, NJ: Rinton Press)
[23] Pollock E and Ceperley D 1987 *Phys. Rev.* B **36** 8343
[24] Winkler R 1995 *Phys. Rev.* B **51** 14395
[25] Filinov A, Peeters F M, Riva C, Lozovik Yu E and Bonitz M 2004 *Few-Body Syst.* **34** 149